# Guest-responsive elastic frustration 'on-off' switching in flexible 2-D spin crossover frameworks

| | |
|---|---|
| Journal: | *Inorganic Chemistry* |
| Manuscript ID | Draft |
| Manuscript Type: | Article |
| Date Submitted by the Author: | n/a |
| Complete List of Authors: | Sciortino, Natasha; The University of Sydney, School of Chemistry<br>ragon, florence; The University of Sydney, School of Chemistry<br>Klein, Maximilian; University of Basel, Catherine Housecroft<br>Housecroft, Catherine; University of Basel, Catherine Housecroft<br>Davies, Casey; University of Otago, Chemistry<br>Jameson, Guy; The University of Melbourne, Bio21: School of Chemistry<br>Chastanet, Guillaume; CNRS, ICMCB<br>Neville, Suzanne; University of New South Wales Faculty of Science, School of Chemistry |
| | |

# Guest-responsive elastic frustration 'on-off' switching in flexible 2-D spin crossover frameworks

Natasha F. Sciortino,[1] Florence Ragon,[1] Y. Maximilian Klein,[2] Catherine E. Housecroft,[2] Casey G. Davies,[3] Guy N. L. Jameson,[3,4] Guillaume Chastanet[5] and Suzanne M. Neville[6*]

[1]School of Chemistry, The University of Sydney, Sydney 2006, Australia.
[2]Department of Chemistry, University of Basel, BPR 1096, Mattenstrasse 24a, CH-4058, Switzerland.
[3]Department of Chemistry & MacDiarmid Institute for Advanced Materials and Nanotechnology, University of Otago, PO Box 56, Dunedin 9054, New Zealand.
[4]School of Chemistry, Bio21 Molecular Science and Biotechnology Institute, 30 Flemington Rd, The University of Melbourne, Parkville, Victoria 3010, Australia.
[5]CNRS, Université de Bordeaux, ICMCB, 87 avenue du Dr. A. Schweitzer, Pessac, F-33608, France.
[6]School of Chemistry, The University of New South Wales, Sydney 2052, Australia.

ABSTRACT: In this study we exploit the flexible nature of porous coordination polymers (PCPs) with integrated spin crossover (SCO) properties to manipulate the multi-stability of spin-state switching profiles. We previously reported the 2-D Hofmann-type framework $[Fe(thtrz)_2Pd(CN)_4]\cdot EtOH,H_2O$ (**1**·EtOH,$H_2O$), *N*-thiophenylidene-4*H*-1,2,4-triazol-4-amine), displaying a distinctive two-step SCO profile driven by extreme elastic frustration. Here, we reveal a reversible release mechanism for this elastic frustration via step-wise guest removal from the parent phase (**1**·EtOH,$H_2O$ → **1**·$H_2O$ → **1**·Ø). Parallel variable temperature structural and magnetic susceptibility measurements reveal a synergistic framework flexing and 'on-off' switching of multistep SCO character concomitant with the onset of guest evacuation. In particular, the two-step SCO properties in **1**·EtOH,$H_2O$ are deactivated such that both the partially solvated (**1**·$H_2O$) and desolvated (**1**·Ø) phases show abrupt and hysteretic one-step SCO behaviors with differing transition temperatures (**1**·$H_2O$: $T_{½}\downarrow$: 215 $T_{½}\uparrow$: 235 K; **1**·Ø: $T_{½}\downarrow$: 170 $T_{½}\uparrow$: 182 K). This 'on-off' elastic frustration switching is also reflected in the light-induced excited spin state trapping (LIESST) properties of **1**·EtOH,$H_2O$ and **1**·Ø, with non-quantitative (*ca*. 50 %, i.e. LS ↔ 1:1 HS:LS) and quantitative (*ca*. 100 %, LS ↔ HS) photo-induced spin state conversion achieved under light irradiation (510 nm at 10 K), respectively. Conversely, the two-step SCO properties are retained in the water saturated phase **1**·$3H_2O$ but with subtle shift in transition temperatures. Comparative analysis of this and related materials reveals the distinct roles that indirect and direct guest-interactions play in inducing, stabilizing and quantifying elastic frustration and the importance of lattice flexible in these porous framework architectures.

## 1. INTRODUCTION

Soft porous crystals, defined as 'porous solids that possess both a highly ordered network and structural transformability', offer a unique set of selective storage and separation functionality.[1] Porous coordination polymers (PCPs) are a characteristic example of such systems as they are highly crystalline, soft and have tunable porous architectures.[2] In 'third generation' PCPs, synergistic framework transformations occur in response to molecular guests resulting in guest-switchable bistability (such as 'gated' porous behaviours) and emergent porous properties.[2,3] Aside from purely structural transformations, other physical attributes, such as electron transfer and spin state, can be perturbed in parallel with PCP flexing.[3] These multi-functioning PCPs have advanced capability due to the strong and synergistic coupling between the host lattice and the guest molecules. A classic example of this is spin state variable molecular sensing such as that observed in the flexible 2-D framework material $[Fe^{II}_2(4,4'\text{-azopyridine})_4(NCS)_4]\cdot EtOH$,[4] which shows a unified spin crossover (SCO)-deactivation and scissor-like flexing of the framework upon guest removal, and the 3-D Hofmann-type framework material $[Fe^{II}(pyrazine)Pt(CN)_4]$,[5] which undergoes a synergistic framework motion and spin state change in response to guests. Alongside exploiting structural flexibility for spin-state molecular sensing, it has been shown that the intrinsic link between host and guest in flexible PCPs can be utilized to tailor SCO characteristics such as thermal hysteresis loop width[6] and multistep spin transitions.[7] For example, the guest-adaptable 2-D Hofmann material $[Fe(proptrz)_2Pd(CN)_4]\cdot 2H_2O$ (proptrz = (*E*)-3-phenyl-*N*-(4*H*-1,2,4-triazol-4-yl)prop-2-yn-1-imine) shows dramatically enhanced cooperativity in the desolvated state as guest evacuation induces optimized host-host interactions through substantial framework mobility.[6c]

Alongside guest sensing applications, Hofmann-type frameworks are known to be a particularly suitable platform for affording multistep SCO transitions as the bimetallic layers can readily support the geometric distortion necessary to house mixed spin state species.[6c,7-8] The geometric malleability of Hofmann frameworks for this purpose is clearly highlighted in the 2-D Hofmann material $[Fe(bztrz)_2\ Pd(CN)_4]\cdot$guest (bztrz = (*E*)-1-phenyl-*N*-(1,2,4-triazol-4-yl)-methanimine),[7b] whereby the number of SCO steps can be directly tuned by guest manipulation, resulting in a broad spectrum of guest-directed multistep properties (i.e., one-, two- and three-step SCO transitions) embodied in the one framework lattice. Alongside this, reversible guest exchange recently documented in the 3-D Hofmann-type framework $[Fe(4\text{-abpt})]\{Ag(CN)_2\}_2]\cdot$guest (4-abpt = 4-amino-3,5-bis(4-pyridyl)-1,2,4-triazole) leads to a variation between four-, two- and one-stepped SCO transitions.[7c] These results support recently developed theoretical models which suggest that elastic frustration, originating from competing long-range ferro- and anti-ferro-elastic interactions, induces multistep SCO transitions.[9] Of relevance here, such interactions are inherently present in the unique framework scaffold of 2-D Hofmann materials of the type $[Fe(R\text{-trz})_2M(CN)_4]$ (where R-trz = 4-functionalized 1,2,4-triazole ligands and M = Pt, Pd) due to the unusual 'asymmetric' mono-dentate binding mode of the R-trz ligand and characteristic arrays of antagonistic host-host host-guest interactions, as illustrated in Figure 1. Reports have highlighted that this general framework platform can be exploited to generate distinctive and emergent multistable SCO properties, including half-,[6c,7b,8f] two-,[8d,7b] three-[7b] and four-step[8g] transitions, hidden SCO and thermal hysteresis,[8f,10] exceptionally wide thermal hysteresis[6c] and guest-tunable multistep SCO switching.[6c,7b]

Motivated by these experimental and theoretical studies on the interplay between host and guest and elastic frustration in flexible frameworks of this type, in this study we expand our exploration of the effect of guest manipulation on elastic frustration to the 2-D Hofmann material $[Fe(thtrz)_2\ Pd(CN)_4]\cdot EtOH,H_2O$ (*N*-thiophenylidene-4*H*-1,2,4-triazol-4-amine; **1**·EtOH,$H_2O$).[8d] This is an important framework platform to explore host-guest effects on as it shows extreme elastic frustration as evidenced by a distinctive two-step SCO behaviour with extended thermal stability of a $HS^{0.5}LS^{0.5}$ species ($\Delta T$ = 120 K) at the intermediate plateau. Notably, variable temperature structural analyses revealed that this exemplary frustrated platform undergoes substantial framework flexing over the two-step spin transition, as supported by an array of host-host and host-guest interactions. Therefore here, we aim to probe if extreme elastic frustration, as observed in $[Fe(thtrz)_2Pd(CN)_4]\cdot EtOH,H_2O$, is intrinsically linked to the flexible framework scaffold or if it is manifested by the interplay between host and guest. In this report, the thermal-induced SCO properties of the partially solvated ($[Fe(thtrz)_2Pd(CN)_4]\cdot H_2O$, **1**·$H_2O$, fully desorbed ($[Fe(thtrz)_2Pd(CN)_4]$, **1**·Ø and water saturated ($[Fe(thtrz)_2Pd(CN)_4]\cdot 3H_2O$, **1**·3$H_2O$ frameworks are explored, as well as the light-induced SCO properties of **1**·EtOH,$H_2O$ and **1**·Ø.

## EXPERIMENTAL SECTION

**General Procedures.** All reagents were commercially available and were used as received. Iron(II) perchlorate was handled carefully and in small amounts to avoid any potential explosions.

**Synthesis.** The complex $[Fe(thtrz)_2Pd(CN)_4]\cdot EtOH,H_2O$ (**1**·EtOH,$H_2O$) was prepared and the identity and purity characterized as per reported procedures.[8d] The partial solvate $[Fe(thtrz)_2Pd(CN)_4]\cdot H_2O$ (**1**·$H_2O$) was attained by heating **1**·EtOH,$H_2O$ to *ca*. 40 °C under dry nitrogen. The desolvate $[Fe(thtrz)_2Pd(CN)_4]$ (**1**·Ø) was attained by heating **1**·EtOH,$H_2O$ or **1**·$H_2O$ to 100 °C under dry nitrogen. The water saturated phase, $[Fe(thtrz)_2Pd(CN)_4]\cdot 3H_2O$ (**1**·3$H_2O$) was prepared by either immersing an air-dried sample of **1**·EtOH,$H_2O$ in neat water for 1-3 days or by thermal desolvation of **1**·EtOH,$H_2O$ followed by immersion in neat water for 1 day.

**Gravimetric analysis.** A sample of **1**·EtOH,$H_2O$ was heated from room temperature to 500 °C at a rate of 1 °C $min^{-1}$ under a dry nitrogen gas flow (20 mL $min^{-1}$) using a TA Instruments Discovery thermogravimetric analyzer (Figure S1). A $H_2O$ sorption isotherm was obtained on **1**·EtOH,$H_2O$ using a Hiden-Isochema intelligent gravimetric analyzer. Prior to adsorption, the sample was outgassed under a vacuum ($10^{-5}$ bar) at 100 °C overnight. The sample was cooled to the analysis temperature (25 °C) and the dry mass recorded. The sample chamber was pressurized to a set pressure and allowed to equilibrate for 240 min before moving to the next pressure point.

**Single Crystal X-ray diffraction.** Variable temperature single crystal X-ray diffraction data and powder X-ray were collected on **1**·EtOH,$H_2O$ with heating to probe the structure upon guest removal. A single crystal was

affixed electrostatically to a MiTeGen loop and heated at 5 K intervals from room temperature to 375 K. Data were collected using a Bruker APEX2 diffractometer equipped with a rotating anode ($\lambda$ = 0.7017 Å), and data integration and reduction were performed using the Bruker software suite.[11] Unit cell data were collected at each 5 K step. The crystal ceased to diffract above 340 K.

**Synchrotron powder X-ray diffraction.** The X-rays (17.03 keV and 0.72808 Å) available at the 17-BM beamline at the APS at Argonne National Laboratory were used in combination with a PerkinElmer area detector with a carbon window to record powder X-ray diffraction patterns. A polycrystalline sample of **1**·EtOH,$H_2O$ was ground into a slurry and loaded into a quartz capillary (0.7 mm diameter) that was open at one end to enable *in situ* desolvation. The sample temperature was controlled using an Oxford Cryosystems open-flow cryostream, and the data were collected in 20 s exposures during continuous ramping over the range 300 – 400 K. The sample was maintained at 400 K for 1 h and then cooled over the range 375-100-300 K at 120 $Kh^{-1}$. This corresponds to the collection of diffraction images at 2 K intervals (for example see Figures S2-3). $LaB_6$ was used as a standard. The raw images were processed using Fit-2D[12] and unit cell analyses were performed within TOPAS.[13]

**Thermal-Induced Magnetic Susceptibility.** Data were collected on a Quantum Design Versalab Measurement System with a vibrating sample magnetometer (VSM) attachment within a small-bore hole cavity. Samples were contained within a polypropylene holder and held within a brass half-tube designed for VSM measurements. Measurements were taken continuously under an applied field of 0.3 T over the temperature range 300 – 50 – 300 K, at a ramp rate of 1 K $min^{-1}$. Step-wise guest removal was carried out within the magnetometer cavity to produce **1**·$H_2O$ and then **1**·Ø, respectively, with heating **1**·EtOH,$H_2O$ to 340 K (followed by measurements over the range of 340–50–300 K) and 400 K (followed by measurements over the range 400 – 50 – 300 K). Data were also collected on samples prepared *ex situ* to the magnetometer resulting the same magnetic data. Data sets were collected on multiple samples to ensure consistency and uniform behavior. Scan rate dependence was previously reported for **1**·EtOH,$H_2O$ (4, 2, 1 and 0.5 K $min^{-1}$)[8d] and we focus here on the 1 K $min^{-1}$ data for the thermally-induced SCO properties.

**Mössbauer Spectroscopy.** Data were recorded on **1**·EtOH,$H_2O$ using a SEE Co. (Science Engineering & Education Co., MN) spectrometer equipped with a closed cycle refrigerator system from Janis Research Co. and SHI (Sumitomo Heavy Industries Ltd.). Data were collected in constant acceleration mode in transmission geometry. The zero velocity of the Mössbauer spectra refers to the centroid of the room temperature spectrum of a 25 μm metallic iron foil. Analysis of the spectra was conducted using the WMOSS program (SEE Co, formerly WEB Research Co. Edina, MN). The sample was first quench cooled to 5.6 K, by quenching the sample in liquid nitrogen before mounting in the Mossbauer instrument. Data were collected at 5.6 K (quench-cooled), 100 K, 170 K and 260 K (Fitted parameters given in Table S1).

**Photo-Induced Magnetic Susceptibility.** Photomagnetic measurements were performed using a set of photodiodes (510 nm at 5 mW $cm^{-2}$ or 830 nm at 3.5 mW $cm^{-2}$), coupled through an optical fibre to the cavity of a MPMS-5S Quantum Design SQUID magnetometer. The optical power at the sample surface was adjusted to prevent local warming effects and irradiation was carried out using different wavelengths to determine the most efficient conditions to reach the highest photoconversion yields. Samples were prepared in a thin layer (~0.1 mg) to promote full penetration of the irradiated light.[14] The sample weight for each measurement was obtained by comparison of the thermal SCO curve with that of a more accurately weighted sample.[14] For both **1**·EtOH,$H_2O$ and **1**·Ø irradiation ($\lambda$ = 510 nm) at 10 K was carried out until photo-saturation, then irradiation was ceased and the temperature increased at a rate of 0.4 K $min^{-1}$ to 100 K. The magnetic susceptibility was then measured every 1 K to determine the $T$(LIESST) value, which was determined as being the extreme of the $\delta\chi_M T/\delta T$ versus T curve.[14-15] The $T$(LIESST) value describes the limiting temperature above which the light-induced magnetic high spin information is erased in a SQUID cavity. In the absence of irradiation, the magnetic susceptibility was also measured over the temperature range 10 – 300 K to follow the thermal spin transition and obtain a low temperature baseline. In addition, reverse LIESST measurements were performed by first attaining complete photo-saturation by irradiation of the sample at 10 K ($\lambda$ = 510 nm), then irradiating with 830 nm light until complete erasure of the photo-induced high spin state (Figure S6). The compound **1**·EtOH,$H_2O$ consists of a yellow polycrystalline solid in a 1:1 ethanol:water solution and the ethanol is rapidly lost if the sample is allowed to dry. Hence, two sample preparations were employed for assessing the photo-magnetic properties of **1**·EtOH,$H_2O$ and **1**·Ø. Firstly, the sample was gently ground and placed as a thin layer directly into the sample holder and secondly, the crystals (un-ground) and a small amount of mother liquor were placed together within a small polyethylene bag and placed within the sample holder. The desolvated phase, **1**·Ø, was attained through the first method upon heating to 375 K and remaining isothermal for one hour within the SQUID cavity.

## RESULTS

**Structure of 1·EtOH,$H_2O$.** The structure of **1**·EtOH,$H_2O$ was previously reported[8d] and we recount it briefly here to aide further discussion. The framework structure of **1**·EtOH,$H_2O$ is characterized by corrugated 2-D Hofmann layers spaced by thtrz ligands (Figure 2(inset)). Substantial layer distortion is evident as directed by antagonistic host-host and host-guest interactions in the interlayer spacing. Within the pores, a distribution of ligand-guest affinities over the thtrz ligand results in dual guest-interaction capacity whereby water molecules are engaged in hydrogen-bonding interactions in proximity to the Hofmann layers ((trz)N…$OH_2$; Pore **A** as depicted in Figure 2(inset)) and ethanol molecules are loosely retained by van der Waals interactions central to the interlayer spacing (Pore **B** as depicted in Figure 2(inset)). Variable temperature single crystal analysis revealed that the two crystallographically distinct $Fe^{II}$ sites (Fe1 and Fe2 as depicted in Figure 2(inset)) undergo a complete spin-state transition in a step-wise manner (i.e, HS-HS, HS-LS, LS-LS, for Fe1-Fe2, respectively) thereby resulting in a two-step SCO profile (Figure 4).

**Two-step guest-removal structure and SCO properties.** Thermogravimetric analysis on **1**·EtOH,$H_2O$ reveals a two-step guest removal progression, i.e., **1**·EtOH,$H_2O$ → **1**·$H_2O$ → **1**·Ø, with the ethanol molecules removed readily at 40 °C followed by the water molecules at 100 °C (Figure S1). The empty framework is stable until 220 °C. Water adsorption measurements on the empty framework reveal a stepped and hysteretic adsorption profile indicative of a flexible PCP undergoing various guest-induced structural transformations (Figure 2).[2] At very low partial pressures (~0.03 $P/P_0$) an abrupt uptake of one water molecule is observed associated with favourable hydrogen bonding (i.e., N(trz)…$OH_2$) interactions at the **A** site (Figure 2(inset)). After this, a gradual uptake of a further two water molecules occur in one broad step (~0.1 – 1 $P/P_0$; **1**·3$H_2O$) reflecting the weaker interaction mode at the **B** site (Figure 2(inset)). Notably, around 0.3 $P/P_0$ the uptake kinetics dramatically slow down suggesting a substantial structural transformation upon insertion/removal of the first water molecule. This hysteretic uptake and release of the secondary water molecules (~0.1 – 1 $P/P_0$) implies a secondary structural transformation. The overall water adsorption-desorption profile indicates that both **A** and **B** guest-docking sites are essential for mutually supporting the distorted 2-D Hofmann topology (Figure 2(inset)).

The structural implication of guest removal was probed using single crystal and powder X-ray diffraction. With heating a single crystal of **1**·EtOH,$H_2O$ the crystallinity abruptly ceases in parallel with ethanol desorption and the single crystal behaviour is not regenerated with guest reintroduction. Therefore, variable temperature synchrotron-based powder X-ray diffraction analysis was conducted on **1**·EtOH,$H_2O$ with heating over the range 270 – 400 K and two distinct structural transformations were revealed (Figure 3). At the onset, the **1**·EtOH,$H_2O$ phase persists over the range 270 – 310 K. Above 310 K a subtle structural deviation emerges, most clearly reflected by the appearance of new peaks (for example at ~10.2 ° Figure 3). The onset temperature of this phase transition (i.e., 37 °C) is consistent with the removal of ethanol from the **B** pore site as per thermogravimetric analysis to produce **1**·$H_2O$. Unit cell analysis on this phase reveals the retention of a triclinic symmetry and similar unit cell parameters to **1**·EtOH,$H_2O$ but with subtle deviation in the triclinic angles (Figure S2-3). This mono-hydrate phase remains stable until *ca*. 360 K where an abrupt shift in peaks occurs alongside a substantial decrease in crystallinity. This is consistent with the removal of water from the **A** pore site to produce **1**·Ø (i.e., 87 °C), and a parallel structural transformation as suggested in the water vapor sorption profile (Figure 2). Unit cell analysis on this phase was not possible due to the substantial peak broadening and intensity reduction.

Temperature-dependent magnetic susceptibility measurements on **1**·EtOH,$H_2O$, **1**·$H_2O$ and **1**·Ø reveal an array of guest-sensitive SCO properties. We previously reported the two-step SCO properties of **1**·EtOH,$H_2O$,[8d] as depicted in Figure 4(a); $T_{½(1)}$↓: 123 $T_{½(2)}$↑: 142 K, ΔT = 19 K; $T_{½(1)}$↓: 228 $T_{½(2)}$↑: 244 K, ΔT = 16 K). Here, removal of the ethanol molecules from the host lattice to form **1**·$H_2O$ sees a conversion to an abrupt and hysteretic one-step SCO transition (Figure 4(b); $T_{½}$↓: 215 $T_{½}$↑: 235 K, ΔT = 12 K). Further guest evacuation to form **1**·Ø retains the one-step hysteretic SCO character (Figure 4(b); $T_{½}$↓: 170 $T_{½}$↑: 182 K, ΔT = 12 K) but results in transition temperatures reduced by around 50 K. Notably, the one-step transition of **1**·Ø is situated approximately central to the intermediate plateau of **1**·EtOH,$H_2O$ (Figure S4). The two-step SCO of **1**·EtOH,$H_2O$ is reversibly regenerated with guest reintroduction but is relatively more gradual (Figure S5). Similarly, the water saturated phase **1**·3$H_2O$ also shows a two-step SCO transition but with subtle deviation in $T_{½}$ values compared to the parent phase **1**·EtOH,$H_2O$ (Figure 4(a); $T_{½(1)}$↓: 123 $T_{½(2)}$↑: 138 K, ΔT = 15 K; $T_{½(1)}$↓: 234 $T_{½(2)}$↑: 251 K, ΔT = 17 K).

**Metastable trapped species via the TIESST and LIESST effect.** $^{57}$Fe Mössbauer spectra of **1**·EtOH,$H_2O$ were recorded at various temperatures starting at 5.6 K upon quench-cooling, and at 100, 170 and 260 K with subsequent heating (Figure 5). For the quench-cooled data (5.6 K) the spectrum exhibits both a quadrupole doublet (46%; $\delta$ = 1.2 mms$^{-1}$ and $\Delta E_Q$ = 3.0 mms$^{-1}$) and singlet (54%; $\delta$ = 0.49 mms$^{-1}$ and $\Delta E_Q$ = 0.12 mms$^{-1}$). These values are characteristic of $Fe^{II}$ in HS and LS state, respectively and reveal a 1:1 HS:LS species at this temperature when quench-cooled. As the temperature is increased to 100 K the thermally trapped species is erased to produce predominantly a LS singlet (90%; $\delta$ = 0.49 mms$^{-1}$ and $\Delta E_Q$ = 0.10 mms$^{-1}$), with a small remnant of the HS doublet (10%; $\delta$ = 1.19 mms$^{-1}$ and $\Delta E_Q$ = 3.02 mms$^{-1}$). This is consistent with magnetic susceptibility data at this temperature and indicates the quench-cooled 1:1 HS:LS species occurs due to thermal trapping via the TIESST effect as discussed below (Figure 6(a)). With further heating to 170 K an approximately equivalent coexistence of a HS quadrupole doublet (47%; $\delta$ = 1.15 mms$^{-1}$ and $\Delta E_Q$ = 2.87 mms$^{-1}$) and LS singlet (53%; $\delta$ = 0.46 mms$^{-1}$ and $\Delta E_Q$ = 0.11 mms$^{-1}$) re-emerge, as per the thermal trapped species. This 1:1 HS:LS species is consistent with the intermediate plateau of the two-step SCO transition as observed by magnetic susceptibility (Figure 4(a)). At 260 K the spectra is characterized by a HS doublet (100%; $\delta$ = 1.11 mms$^{-1}$ and $\Delta E_Q$ = 2.26 mms$^{-1}$) in line with the complete HS character anticipated at this temperature (Figure 4(a)).

The evolution of a thermally trapped 1:1 HS:LS species in **1**·EtOH,$H_2O$ was also monitored by magnetic susceptibility measurements via rapid immersion of the sample into the SQUID cavity at 10 K (Figure 6(a)). At 10 K with quench-cooling, a $\chi_M T$ value of *ca*. 0.81 cm$^3$mol$^{-1}$ K is attained which increases to a maximum of 1.33 cm$^3$mol$^{-1}$ K by 55 K. The marked increase with heating over the range 10 – 55 K is associated with zero-field splitting of the HS $Fe^{II}$ centers. The maximum low temperature trapping value indicates a thermally-trapped-conversion yield of 45% HS $Fe^{II}$ ions, which is commensurate with that observed by Mössbauer spectroscopy. Beyond 60 K, the approximately 1:1 HS:LS TIESST species relaxes to the LS state with a characteristic *T*(TIESST) temperature of 69 K, as defined by the minima of the $\delta\chi_M T/\delta T$ curve (Figure 6(a): inset).

Given the thermal trapping effects observed in **1**·EtOH,$H_2O$ via the TIESST effect, the effect of light-irradiation through the LIESST effect was also examined. After slow cooling to 10 K, the sample was irradiated with 510 nm light resulting in a rapid increase in $\chi_M T$ values to *ca*. 0.78 cm$^3$mol$^{-1}$ K indicating LIESST activity. Further heating in the absence of irradiation results in a further increase in $\chi_M T$ values to a maximum of 1.11 cm$^3$mol$^{-1}$ K by 45 K (Figure 6(a)). As per the TIESST data, this increase is due to zero-field splitting of the HS $Fe^{II}$ centers. The maximum light-induced-conversion yield attained is 40% which is slightly diminished compared to the TIESST species, likely owing to variation in trapping efficiency achieved by the distinct methodologies. Subsequent heating above 45 K results in a complete relaxation to the LS state and a characteristic *T*(LIESST) value of 65 K as

defined by the minima of the $\delta\chi_M T/\delta T$ curve. Alongside heat application, the photo-induced species can also be erased by irradiation at 830 nm via the reverse-LIESST effect (Figure S6). Structural analysis of both the TIESST and LIESST species were not possible due to loss of crystallinity. The subtle difference in $T$(TIESST) and $T$(LIESST) values for **1**·EtOH,$H_2O$ (i.e., 69 and 65 K, respectively) suggests that perhaps distinct metastable 1:1 HS:LS species are achieved by the TIESST and LIESST processes but may also be due to the noted variation in trapping efficiencies of the two methodologies.

The photomagnetic properties of **1**·Ø were also investigated by irradiating a sample with 510 nm light revealing a rapid increase in $\chi_M T$ values to 2.2 $cm^3$ K $mol^{-1}$ at 10 K (Figure 6(b)). With heating, the photo-induced trapped species, as per **1**·EtOH,$H_2O$, shows an increase in $\chi_M T$ values to a maximum of *ca*. 3.22 $cm^3mol^{-1}$ K at 45 K associated with zero-field splitting of the $Fe^{II}$ centers. The maximum light-induced-conversion yield attained is 95 % indicating a near quantitative trapping of a metastable HS species by the LIESST effect for **1**·Ø. Further heating above 45 K results in the LIESST HS species being erased and a characteristic $T$(LIESST) value of 63 K as defined by the minima of the $\delta\chi_M T/\delta T$ curve.

## DISCUSSION

The framework material **1**·EtOH,$H_2O$ represents the first in a series of targeted 2-D Hofmann materials which incorporate systematically functionalized 1,2,4-triazole ligands.[6c,7b,8d,f,g,i,10a,b] Our focus is on delivering facile systematic chemical variation into the interlayer spacing of these 2-D frameworks by targeting 1,2,4-triazole ligands functionalized with a range of aromatic and hydrogen-bonding characteristics (see Figure 1). This facile approach has afforded a range of materials of the general formula $[Fe(R\text{-}trz)_2M(CN)_4]\cdot x$guest (M = Pt, Pd) with a wide range of remarkable functional group- and guest-dependent structural and SCO features. In all of the $[Fe(R\text{-}trz)_2M(CN)_4]\cdot x$guest examples thus far reported the emerging theme is that of SCO properties dictated by elastic frustration arising from this unique 2-D Hofmann platform (i.e, the monodentate 1,2,4-triazole binding mode which intrinsically generates competing ferro- and antiferro-elasticity; see Figure 1).[9] Indeed, the structure and magnetic properties of **1**·EtOH,$H_2O$ are exemplary in this respect, whereby structurally distinct regions of antagonistic host-host and host-guest interactions (Figure2:inset) support the emergence of a complete two-step SCO transition (Figure 4(a)).[8d] Contrasting this, the closely related materials $[Fe(trz\text{-}py)_2M(CN)_4]\cdot 3H_2O$ (trz-py = 4-(2-pyridyl)-1,2,4,4*H*-triazole, M = Pd,[8f] Pt[8i]), $[Fe(bztrz)_2Pd(CN)_4]\cdot$EtOH,$H_2O$[7b] and $[Fe(proptrz)_2Pd(CN)_4]\cdot 2H_2O$[6c] exhibit "half"-SCO transitions, where one of two crystallographically distinct $Fe^{II}$ sites undergo a spin transition, the other remaining indefinitely "trapped" in the HS state. It has, however, been shown that light-irradiation[8f,10b] and guest-exchange[6c,7b] are perturbation methods that can be employed to overcome elastic frustration "trapping" to produce complete, yet still multistep transitions. Further to this, a recent study on $[Fe(proptrz)_2Pd(CN)_4]\cdot 2H_2O$[6c] has revealed a complete erasure of multistep character concurrent with guest removal; this provided the first indication that elastic frustration may indeed not be intrinsic to this general framework platform but reliant on the synergy between host-host and host-guest interactions. Further supporting this is the 'on/off' multistep switching achieved here in **1**·EtOH,$H_2O$ upon partial and complete guest removal. Adding further insight into the drivers for elastic frustration, the observation of a one-step SCO transition in the mono-hydrate phase (**1**·$H_2O$), where all other guest modulated phases previously have retained multistep character, indicates that elastic frustration evolution is more complex than merely the co-existence of host-host and host-guest interactions and perhaps other structural factors, such as lattice flexibility, must also be considered. Of further consideration in this respect is the role of asymmetric host-host interactions; further to studies on 2-D Hofmann frameworks, two recent reports on four-step SCO transitions in porous 3-D Hofmann frameworks have further highlighted the important role they provide in supporting multistep SCO.[7c,8e]

To probe more quantitatively the 'on/off' elastic frustration switching achieved here with partial and complete guest perturbation, we now consider the respective influence of the two distinct guest docking sites within the pores (**A** and **B**; Figure 2:inset). From a structural perspective, within the general family $[Fe(R\text{-}trz)_2M(CN)_4]\cdot x$guest (M = Pt, Pd) there are two distinct categories: 1) those with approximately planar Hofmann layers[6c,10a] and 2) those with distorted non-planar Hofmann layers.[7b,8d,f,g,i] In the majority of cases the Hofmann layers show substantial undulation directed and stabilized by the competition between host-host and host-guest interactions (Figure 2:inset). Layer undulation provides a platform for the distinction of multiple structurally unique $Fe^{II}$ sites which undergo spin-state transition at different temperatures, resulting in multistep transitions. Further to this, guest modulation studies on $[Fe(bztrz)_2Pd(CN)_4]\cdot$guest[7b] highlight that the undulating layers afford two distinct guest docking sites in the pores (**A** and **B**) and that guest exchange at the **B** site enables subtle tuning of elastic frustration, in this case, in the form of half-, two- and three-step spin transitions embodied in the one framework scaffold. However, a comprehensive study on guest removal effects at both the **A** and **B** sites was inhibited due to loss of SCO character with guest evacuation. Here, the retention of SCO character in the apohost and partially desolvated phase facilitates a broad comparative analysis of guest exchange and removal effects at each of the guest sites. An overview of the relative guest occupancy at the **A** and **B** guest docking sites and overall magnetic outcome for this and other analogues in this general family with undulating Hofmann layers are collated in Table 1. From this, overall, it is evident that elastic frustration is maintained only when guest molecules reside in the **B** site (i.e., **1**·EtOH,$H_2O$ and **1**·3$H_2O$), however, when the **B** pore site is vacant (i.e., **1**·$H_2O$ and **1**·Ø) elastic frustration is released. This confirms that the primary role of the **B** site guest molecules is in supporting elastic frustration which is tuned via the relative steric impact of the respective molecular guests. On the other hand, the retention of one-step character and substantially increased transition temperature of **1**·$H_2O$ versus **1**·Ø (Figure 4(b)), indicates that the **A** pore site influences spin-state communication; this is reasonable considering its close proximity to the $Fe^{II}$ sites.

Alongside assessing the effect of guest occupancy on elastic frustration, also emerging from this comparative analysis (Table 1) is that retention of SCO character with complete guest removal is unique for **1**·guest, with respect to those examples with undulating Hofmann layers. Indeed, within this general family there are only two previously reported examples of SCO activity retained with complete guest removal, $[Fe(proptrz)_2Pd(CN)_4]\cdot 2H_2O$[6c] and $[Fe(thiome)_2Pd(CN)_4]\cdot 2H_2O$, thiome = 4-[(E)-2-(5-methyl-2-thienyl)vinyl]-1,2,4-triazole)[10a] and both of which, notably, display (approximately) planar Hofmann layers. Whilst single crystal structural analysis was not possible on **1**·$H_2O$ and **1**·Ø, variable temperature powder diffraction data and water vapor adsorption measurements both indicate substantial structural transformations upon guest removal from **1**·EtOH,$H_2O$. Therefore, it is likely that removal of the structural stabilizing pore **B** guests from **1**·EtOH,$H_2O$ may drive a robust structural transformation to achieve Hofmann layer planarity. Further supporting this hypothesis, layer planarity would support the unification of crystallographically distinct $Fe^{II}$ sites thereby enabling a cooperative one-step spin-state transition of $Fe^{II}$ sites. This is also consistent with the one-step spin transitions emergent in the desolvated forms of $[Fe(proptrz)_2Pd(CN)_4]$ and $[Fe(thiome)_2Pd(CN)_4]$. Overall, comparison within this grown family of related materials reveals that the capacity to retain structural stability and SCO character in the absence of guests is most likely driven by each frameworks unique robust capacity to adapt to structural changes, in particular through the presence of secondary supporting interactions, such as S…S interaction in the case of **1**·EtOH,$H_2O$ and $[Fe(thiome)_2Pd(CN)_4]$ and aromatic interaction in $[Fe(proptrz)_2Pd(CN)_4]$.

Beyond assessing the impact of guest-modulation on the thermal SCO properties, photomagnetic characterizations on the mixed guest phase (**1**·EtOH,$H_2O$) and empty framework (**1**·Ø) reveal that elastic frustration effects are reflected in the LIESST properties. As the thermal SCO of **1**·EtOH,$H_2O$ is two-step in character, there are two main ways that the LIESST profile could present: 1) as a

quantitative metastable HS state with a two-step relaxation reflecting both steps of the thermal SCO and 2) as a metastable 1:1 HS:LS state with a one-step relaxation process reflecting the lower temperature thermal SCO step. We observe here a *ca*. 50% trapping efficiency under the application of light-irradiation at low temperature indicating the presence of a metastable 1:1 HS:LS species. Through comparing $T_{½}$ and $T$(LIESST) values using the established relationship $T$(LIESST) = $T_0$ – 0.3$T_{½}$, where $T_0$ represents an empirical measure of the degree of cooperativity (defined as 100 K for unidentate ligands, 120 K for bidentate ligands, 150 K for meridional ligands and 200 K for network materials)[14,15] **1**·EtOH,$H_2O$ is placed in the $T_0$ = 100 K family. This placement is based on the low temperature SCO step and confirms that the high temperature SCO step is not LIESST active. Moreover this highlights that even though the SCO centers are linked into a 2-D network through coordination bonds and communicate in a 3-D manner through supramolecular interactions, the $Fe^{II}$ ions behave as if surrounded by monodentate ligands, which to a first approximation reflects reality.[8a,g,16] In contrast to **1**·EtOH,$H_2O$, the one-step complete SCO character of **1**·Ø is reflected by a one-step quantitative trapping of a metastable HS species upon light-irradiation. As for **1**·EtOH,$H_2O$, the $T_{½}$ and $T$(LIESST) values place **1**·Ø also in the $T_0$ = 100 K family; this is not surprising given the framework connectivity is unchanged with guest perturbation, however, we might anticipate that the $T$(LIESST) values would differ more dramatically between **1**·EtOH,$H_2O$ and **1**·Ø given their distinctly different $T_{½}$ values. The reason for this is unknown at this time and as LIESST studies involving guest modulation are rare,[15b,7] and have not previously been conducted on porous MOF-type species, further studies are required to gain a broader understanding. However, it is known that overall Hofmann materials tend to show LIESST activity that is weakly sensitive to $T_{½}$ values which has previously been proposed to be due to the unique Hofmann topology construct which is composed of strong cooperative pathways (within the 2-D layers) which are unable to communicate in a true 3-D manner owing to weak cooperativity between layers.[16b]

## CONCLUSIONS

In summary, we present a diverse range of guest-adaptable SCO properties in the 2-D Hofmann phase $[Fe(thtrz)_2Pd(CN)_4]$·guest (guest = {EtOH,$H_2O$}, $3H_2O$, $H_2O$ and Ø) which forms part of a growing family of related materials with underlying elastic frustration effects. The 2-D Hofmann materials within this general family display characteristic arrays of antagonistic host-host and host-guest interactions which mutually support varying degrees of elastic frustration and drive the emergence of multistep SCO transitions. Previous studies have indicated that this unique design platform imparts intrinsic elastic frustration on the framework scaffold and have furthermore shown that subtle guest-induced perturbation to these antagonistic interactions can result in remarkable variation to multistep SCO character. Here, through exploiting the substantial guest-adaptability of $[Fe(thtrz)_2Pd(CN)_4]$·guest four distinct guest-loaded phases have been produced which encompass both two- and one-stepped behaviors. This primarily highlights that multistep switching is not intrinsic to these materials and may be entirely extinguished under specific circumstances. Furthermore, collective rational analysis of the pore content distribution and overall SCO properties of this and other related complexes has revealed that the weakly interacting internal guests act to stabilize elastic frustration and can be exploited to tune the degree of elastic frustration, largely through steric considerations. It is further evidenced that strongly interacting guests close to the Hofmann layers provide a cooperativity enhancement. Finally, in this respect, this study has confirmed that in this growing family of related porous 2-D framework materials alongside tailored host-host and host-guest interactions (i.e., ligand functionalization and/or guest variation), lattice flexibility is another tool that must be considered in modulating and assessing elastic frustration effects. With this broader understanding of the relative influence of various structural parameters, new materials can be specifically targeted with strategically designed superior lattice flexibility in order to drive and tailor more complex and potentially emergent spin-state ordering effects. Alongside

achieving greater diversity, such studies will broaden our understanding of the mechanism for propagation of elastic frustration in three-dimensions, not only through the $[FeM(CN)_4]$ planes. In this sense 2-D networks are ideal candidates since the in-between plane direction can act as the flexible axis of the whole network, with a parallel enhanced molecular sensing effect anticipated.

## ASSOCIATED CONTENT

### Supporting Information

The Supporting Information is available free of charge on the ACS Publications website.

Additional characterization (gravimetry), powder X-ray diffraction, magnetic measurements and Mössbauer parameters.

## AUTHOR INFORMATION

### Corresponding Author

*Email: s.neville@unsw.edu.au

### Notes

The authors declare no competing financial interest.

## ACKNOWLEDGMENTS

The Australian Research Council is thanked for providing Discovery Grants and Research Fellowships to support this work at the University of Sydney and The University of New South Wales. The University of Otago, the MacDiarmid Institute and The University of Melbourne and thanked for financial support. The University of Bordeaux, the CNRS, the Aquitaine Region are thanked for providing support. Access and use of the facilities of the APS was supported by the U.S. Department of energy, Office of Science, Office of Basic Energy Sciences (Contract DE-AC02-06CH11357). Travel to the APS was funded by the International Synchrotron Access Program (ISAP) managed by the Australian Synchrotron and funded by the Australian Government. The University of Basel is acknowledged for support. We thank Dr Gregory J. Halder, Prof Cameron J. Kepert and Katrina A. Zenere for discussions and assistance.

## REFERENCES

(1) Horike, S.; Shimomura, S.; Kitagawa S. Soft porous crystals. *Nat. Chem.* **2009**, 695-704.

(2) Kitagawa, S.; Kitaura, R.; Noro, S.-I. Functional porous coordination polymers. *Angew. Chem. Int. Ed.* **2004**, 43, 2334-2375.

(3) Sato, O. Dynamic molecular crystals with switchable physical properties. *Nat. Chem.* **2016**, 644-656.

(4) Halder, G. J.; Kepert, C. J.; Moubaraki, B.; Murray, K. S.; Cashion, J. D. Guest-dependent spin crossover in a nanoporous molecular framework material. *Science* **2002**, 298, 1762-1765.

(5) Ohba, M.; Yoneda, K.; Agustí, G.; Muñoz, C.; Gaspar, A. B.; Real, J. A.; Yamasaki, M.; Ando, H.; Nakao, Y.; Sakaki, S.; Kitagawa, S. Bidirectional Chemo-Switching of Spin State in a Microporous Framework. *Angew. Chem. Int. Ed.* **2009**, 48, 4767-4771.

(6) (a) Neville, S. M.; Halder, G. J.; Chapman, K. W.; Duriska, M. B.; Moubaraki, B.; Murray, K. S.; Kepert, C. J. Guest tunable structure and spin crossover properties in a nanoporous coordination framework material. *J. Am. Chem. Soc.* **2009**, 131, 12106-12108 (b) Southon, P. D.; Lui, L.; Fellows, E. A.; Price, D. J.; Halder, G. J.; Chapman, K. W.; Moubaraki, B.; Murray, K. S.; Létard, J.-F.; Kepert, C. J. Dynamic interplay between spin-crossover and host-guest function in a nanoporous metal-organic framework material. *J. Am. Chem. Soc.* **2009**, 131, 10998-11009 (c) Zenere, K. A.; Duyker, S. G.; Trzop, E.; Collet, E.; Chan, B.; Doheny, P. W.; Kepert, C. J.; Neville, S. M. Increasing spin crossover cooperativity in 2D Hofmann-type materials with guest molecule removal. *Chem. Sci.* **2018**, DOI: 10.1039/c8sc01040d.

(7) (a) Bao, X.; Shepherd, H. J.; Salmon, L.; Molnár, G.; Tong, M.-L.; Bousseksou, A. The effect of an active guest on the spin crossover phenomenon *Angew. Chem. Int. Ed.* **2013**, 52, 1198-1202 (b) Murphy, M. J.; Zenere, K. A.; Ragon, F.; Southon, P. D.; Kepert, C. J.; Neville, S. M. Guest programmable multistep spin crossover in a porous 2-D Hofmann-type material. *J. Am. Chem. Soc.* **2017**, 139, 1330-1335; (c) Liu, W.; Peng, Y.-Y.; Wu, S.-G.; Chen, Y.-C.; Hoque, M. N.; Ni, Z.-P.; Chen, X.-M.; Tong, M.-L. Guest-switchable multi-step spin transitions in an amine-functionalised metal-organic framework, *Angew. Chem. Int. Ed.* **2017**, 56, 14982-14986.

(8) (a) Sciortino, N. F.; Scherl-Gruenwald, K. R.; Chastanet, G.; Halder, G. J.; Chapman, K. W.; Létard, J.-F.; Kepert, C. J. Hysteretic three-step spin crossover in a thermo- and photochromic 3D pillared Hofmann-type metal-organic framework. *Angew. Chem. Int. Ed.* **2012**, 51, 10154-10158; (b) Ohtani, R.; Arai, M.; Hori, A.; Takata, M.; Kitao, S.; Seto, M.; Kitagawa, S.; Ohba, M. Modulation of spin-crossover behavior in an elongated and flexible Hofmann-type porous coordination polymer. *J. Inorg. Organomet. Polym,* **2013**, 23, 104-110; (c) Ohtani, R.; Arai, M.; Ohba, H.; Hori, A.; Takata, M.; Kitagawa, S.; Ohba, M. Modulation of the interlayer structures and magnetic behavior of 2D spin-crossover coordination polymers $[Fe^{II}(L)_2Pt^{II}(CN)_4]$. *Eur. J. Inorg. Chem.* **2013**, 738-744; (d) Klein, Y. M.; Sciortino, N. F.; Ragon, F.; Housecroft, C. E.; Kepert, C. J.; Neville, S. M. Spin crossover intermediate plateau stabilization in a flexible 2-D Hofmann-type coordination polymer. *Chem. Commun.* **2014**, 50, 3838-3840; (e) Clements, J. E.; Price, J. R.; Neville, S. M.; Kepert, C. J. Hysteretic four-step spin crossover within a three-dimensional porous Hofmann-like material. *Angew. Chem. Int. Ed.*, **2016**, 55, 15105-15109; (f) Milin, E.; Patinec, V.; Triki, S.; Bendeif, E.-E.; Pillet, S.; Marchivie, M.; Chastanet, G.; Boukheddaden, K. Elastic frustration triggering photoinduced hidden hysteresis and multistability in a two-dimensional photoswitchable Hofmann-like spin-crossover metal-organic framework. *Inorg. Chem.* **2016**, 55(22), 11652-11661; (g) Sciortino, N. F.; Zenere, K. A.; Corrigan, M. E.; Halder, G. J.; Chastanet, C.; Létard, J.-F.; Kepert, C. J.; Neville, S. M. Four-step iron(II) spin state cascade driven by antagonistic solid state interactions. *Chem. Sci.*, **2017**, 8, 701-707; (h) Liu, F.-L.; Li, D.; Su, L.-J.; Tao, J. Reversible three equal-step spin crossover in an iron(II) Hofmann-type metal-organic framework, *Dalton Trans*. **2018**, 47, 1407-1411; (j) Liu, F.-L.; Tao, J.; Hysteretic two-step spin-crossover behavior in two two-dimensional Hofmann-type coordination polymers. *Chem. Eur. J.* **2017**, 23, 18252-18257; (i) Fourati, H.; Milin, E.; Slimani, A.; Chastanet, G.; Abid, Y.; Triki, S.; Boukheddaden, K. Interplay between crystal's shape and spatiotemporal dynamics in a spin transition material. *Phys. Chem. Chem. Phys*. **2018**, 20, 10142-10154.

(9) Paez-Espejo, M.; Sy, M.; Boukheddaden, K. Elastic frustration causing two-step and multistep transitions in spin-crossover solids: emergence of complex antiferroelastic structures. *J. Am. Chem. Soc.* **2016**, 138, 3202-3210.

(10) (a) Sciortino, N. F.; Ragon, F.; Zenere, K. A.; Southon, P. D.; Halder, G. J.; Chapman, K. W.; Pineiro-Lopez, L.; Real, J. A.; Kepert, C. J.; Neville, S. M. Exploiting pressure to induce a "guest-blocked" spin transition in a framework material. *Inorg. Chem.* **2016**, 55, 10490-10498; (b) Ndiaye, M. M.; Pillet, S.; Bendeif, E.-E.; Marchivie, M.; Chastanet, G.; Boukheddaden, K.; Triki, S. Hidden hysteretic behavior of a paramagnetic iron(II) network revealed by light irradiation. *Eur. J. Inorg. Chem.* **2018**, 305-313.

(11) APEX II Software Package **2005**, Madison, WI., Bruker AXS Inc.

(12) Hammersley, A. P. FIT2D: a multi-purpose data reduction, analysis and visualization program. *J. Appl. Crystallogr.* **2016**, 49, 646−652.

(13) TOPAS, version 4.2; Bruker Analytical Instruments Inc.: Madison, WI, **2009**.

(14) (a) J.-F. Létard; P. Guionneau; L. Rabardel; J. A. K. Howard; A. E. Goeta; D. Chasseau; Kahn, O. Structural, magnetic and photomagnetic studies of a mononuclear iron(II) derivative exhibiting an exceptional abrupt spin transition. Light-induced thermal hysteresis phenomenon. *Inorg. Chem.* **1998**, *37*, 4432-4441; (b) Létard, J.-F. Photomagnetism of iron(II) spin crossover complexes – the T(LIESST) approach. *J. Mater. Chem.* **2006**, *16*, 2550-2559.

(15) (a) Létard, J.-F.; Capes, L.; Chastanet, G.; Moliner, N.; Létard, S.; Real, J. A.; Kahn, O. Critical temperature of the LIESST effect in iron(II) spin crossover compounds. *Chem. Phys. Lett.* **1999**, *313*, 115-120; (b) Marcen, S.; Lecren, L.; Capes, L.; Goodwin, H. A.; Létard, J.-F. Critical temperature of the LIESST effect in a series of hydrated and anhydrous complex salts $[Fe(bpp)_2]X_2$. *Chem. Phys. Lett.* **2002**, 358(1,2), 87-95. (c) Hauser, A. Light-induced spin crossover and the high-spin→low-spin relaxation. *Top. Curr. Chem.* **2004**, *234*, 155-198; (d) Létard, J. F.; Guionneau, P.; Nguyen, O.; Costa, J. S.; Marcén, S.; Chastanet, G.; Marchivie, M.; Goux-Capes, L. A guideline to the design of molecular-based materials with long-lived photomagnetic lifetimes. *Chem. Eur. J.* **2005**, *11*, 4582-4589.

(16) (a) Martínez, V.; Castillo, Z. A.; Muñoz, M. C.; Gaspar, A. B.; Etrillard, C.; Létard, J.-F.; Terekhov, S. A.; Bukin, G. V.; Real, J. A. Thermal-, pressure- and light-induced spin-crossover behavior in the two-dimensional Hofmann-like coordination polymer $[Fe(3\text{-}Clpy)_2Pd(CN)_4]$. *Eur. J. Inorg. Chem.* **2013**, 5-6, 813-818; (b) Sciortino, N. F.; Neville, S.

M.; Létard, J.-F.; Moubaraki, B.; Murray, K. S.; Kepert, C. J. Thermal- and light-induced spin-crossover bistability in a disrupted Hofmann-type 3D framework. *Inorg. Chem.*, **2014**, 53(15), 7886-7893.

(17) Amoore, J. J. M; Neville, S. M.; Moubaraki, B.; Iremonger, S. S.; Murray, K. S.; Létard, J.-F.; Kepert, C. J. Thermal- and light-induced spin crossover in a guest-dependent dinuclear iron(II) system. *Chem. Eur. J.* **2010**, 16(6), 1973-1982.

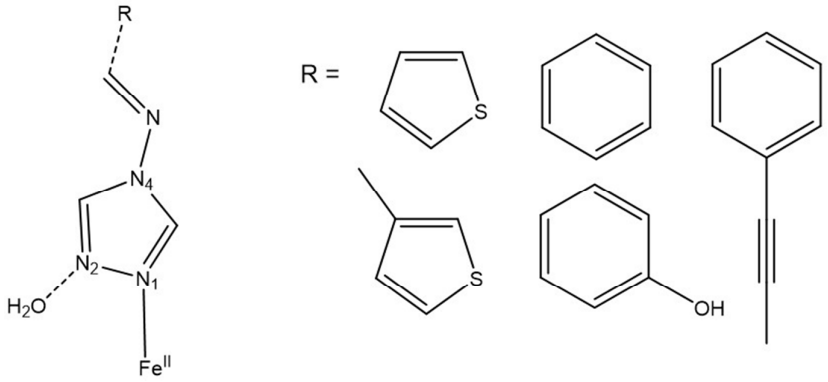


**Figure 1**. Illustration of the monodentate $Fe^{II}$-$N_1$(triazole) binding and host-guest ($N_2$(triazole)…$H_2O$) interactions observed in reported 2-D Hofmann frameworks of the type $[Fe(R\text{-}trz)_2Pd(CN)_4]$, where R-trz represents various $N_4$-functionalized 1,2,4-triazole ligands as shown.

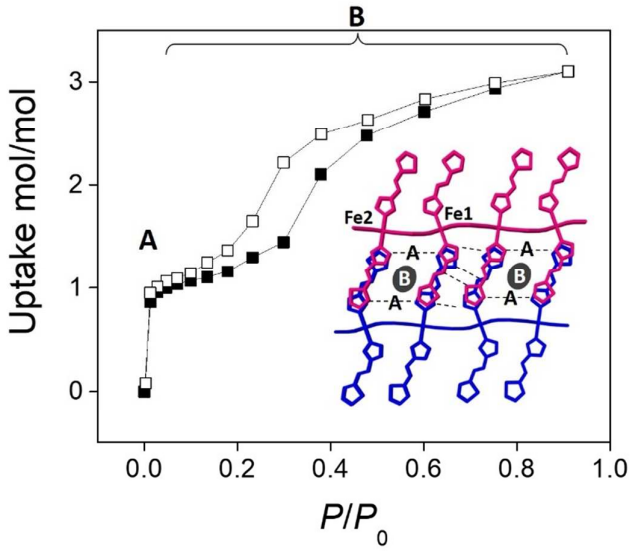


**Figure 2.** Water vapor adsorption (closed squares) and desorption (open squares) isotherms for **1** at 25 °C. Inset: Two neighboring layers (pink and blue) in the framework structure of **1**·EtOH,$H_2O$ highlighting the two distinct guest docking sites (**A** and **B**), the host-host and host-guest interactions (---) and the crystallographically distinct $Fe^{II}$ sites (Fe1 and Fe2).

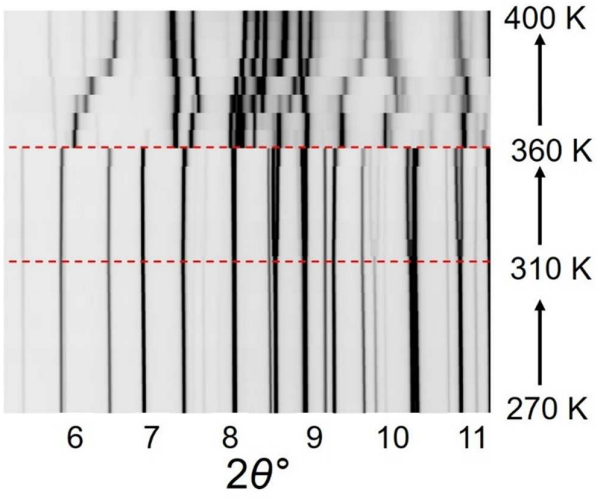


**Figure 3.** Variable temperature synchrotron powder X-ray diffraction data single peak evolution over the range 5 – 11° and 270 – 400 K. The phase **1**·EtOH,$H_2O$ is present over the range 270 – 310 K, the **1**·$H_2O$ phase over the range 310 – 360 K and the **1**·Ø phase over the range 360 – 400 K. The red dotted lines indicate temperatures of phase transition between the solvates.

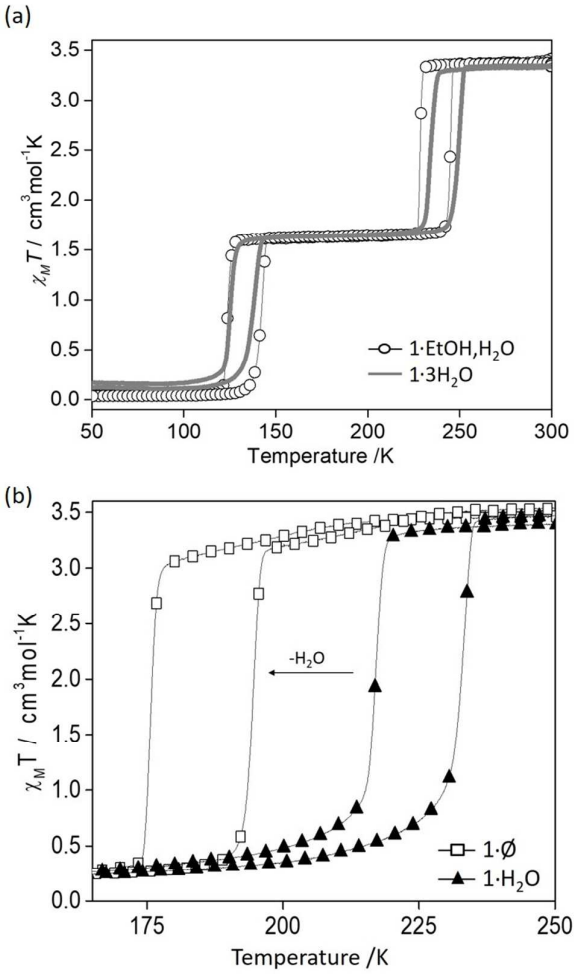


**Figure 4.** Guest-sensitive variable temperature magnetic susceptibility data (scan rate = 1 K min$^{-1}$) for (a) **1**·EtOH,$H_2O$ (○) and **1**·3$H_2O$ (⁻) and (b) **1**·$H_2O$ (▲) and **1**·Ø (□).

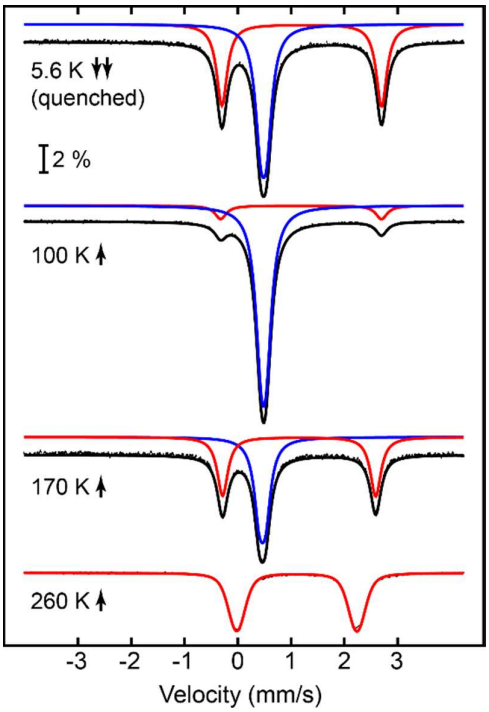


**Figure 5.** Variable temperature $^{57}$Fe Mössbauer spectra of **1**·EtOH,$H_2O$ recorded at 5.6 K with quench cooling and 100, 170 and 260 K with slow heating. The intensity resonance signals of the thermally trapped (5.6 K) and intermediate plateau (170 K) are close to 1:1 for HS:LS. At 100 K near complete LS character is observed and complete HS character at 260 K.

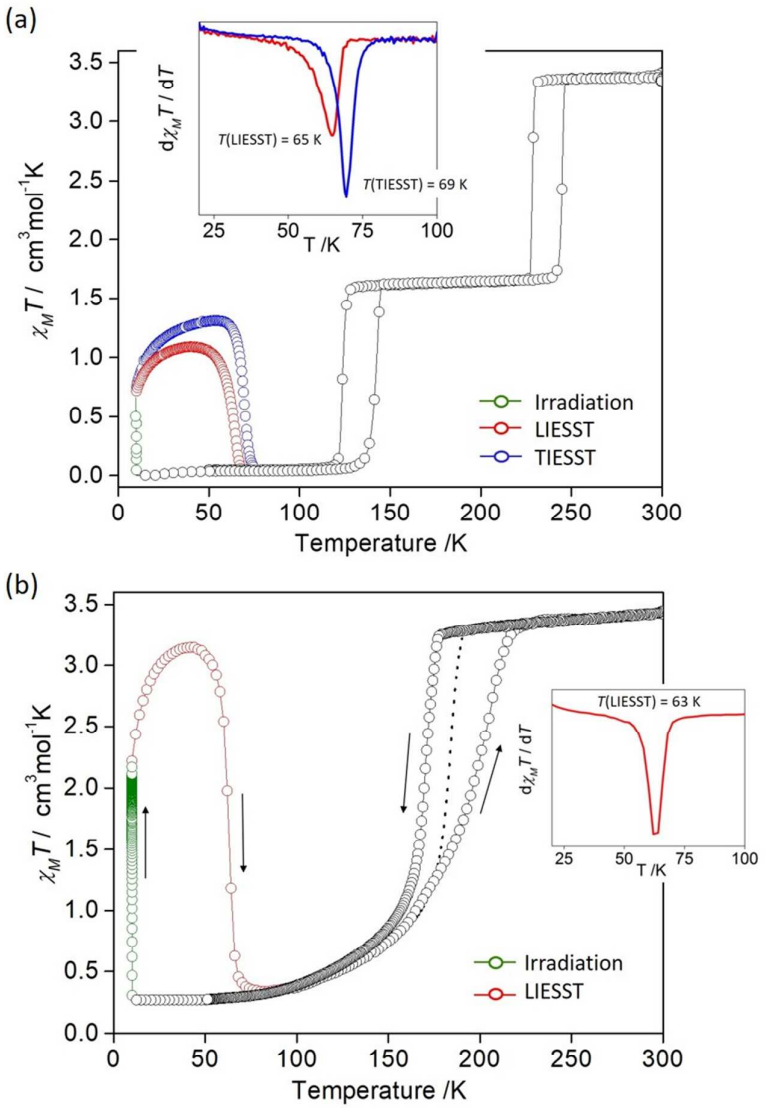


**Figure 6.** (a) Thermal- and light-induced metastable HS state trapping properties of **1**·EtOH,$H_2O$ (scan rate = 0.4 K min$^{-1}$) showing: (1) the thermally induced two-step SCO (black circles); (2) with quench cooling to 10 K and subsequent heating over the range 10 – 100 K (blue circles) and (3) with light irradiation (510 nm, green circles) at 10 K (red triangles) and subsequent heating over the range 10 – 100 K (red circles). Inset: Derivative of the thermal trapping relaxation ($\delta\chi_M T/\delta T$) indicating a $T$(TIESST) value of 69 K (blue) and derivative of the light-induced relaxation ($\delta\chi_M T/\delta T$) indicating a $T$(LIESST) value of 65 K (red). (b) Light-induced metastable HS state trapping properties of **1**·Ø (scan rate = 0.4 K min$^{-1}$) showing: (1) the thermally induced one-step SCO (black circles); (2) with light irradiation (510 nm, green circles) at 10 K (red triangles) and subsequent heating over the range 10 – 100 K (red circles). Inset: Derivative of the thermal trapping relaxation ($\delta\chi_M T/\delta T$) indicating a $T$(TIESST) value of 63 K (red). Arrows indicate direction of measurement. Dotted line is a visual guide showing the thermal SCO heating profile attained without LIESST.

**Table 1**: Summary of the relative pore **A** and pore **B** occupancy and SCO characteristics of various [Fe(R-trz)$_2$M(CN)$_4$]·*x*guest (M = Pt, Pd) 2-D Hofmann frameworks with undulating layers

| **complex** | **A contents** | **B contents** | **# SCO steps** | **multistep** |
|---|---|---|---|---|
| [Fe(thtrz)$_2$Pd(CN)$_4$]·EtOH,H$_2$O[8d] | H$_2$O | EtOH | 2 | Y |
| [Fe(thtrz)$_2$Pd(CN)$_4$]·H$_2$O | H$_2$O | - | 1 | N |
| [Fe(thtrz)$_2$Pd(CN)$_4$] | - | - | 1 | N |
| [Fe(thtrz)$_2$Pd(CN)$_4$]·3H$_2$O | H$_2$O | 2H$_2$O | 2 | Y |
| [Fe(bztrz)$_2$Pd(CN)$_4$]·EtOH,H$_2$O[7b] | H$_2$O | EtOH | ½ | Y |
| [Fe(bztrz)$_2$Pd(CN)$_4$]·~2H$_2$O[7b] | H$_2$O | ~H$_2$O | 3 | Y |
| [Fe(bztrz)$_2$Pd(CN)$_4$]·3H$_2$O[7b] | H$_2$O | 2H$_2$O | 2 | Y |
| [Fe(trz-py)$_2$Pt(CN)$_4$]·3H$_2$O[8f] | H$_2$O | 2H$_2$O | ½ | Y |

TOC graphical abstract

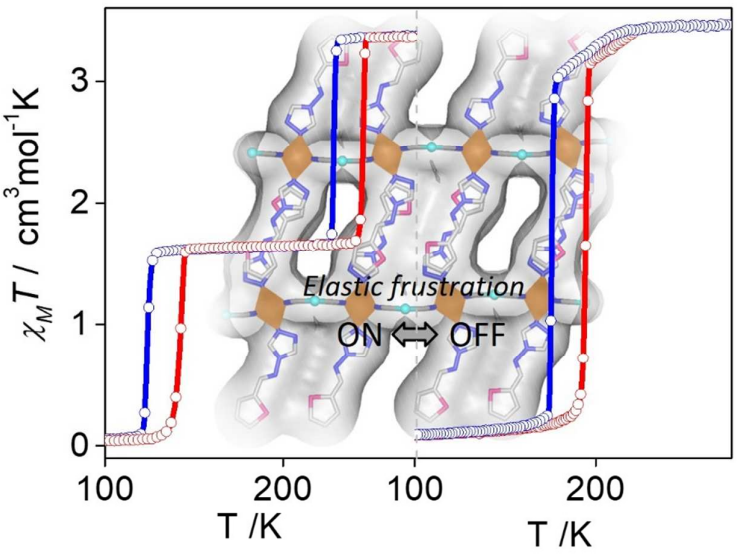


Flexible porosity enables multistep spin crossover switching to be systematically turned ON and OFF with manipulation of the pore contents in a 2-D Hofmann framework materials